

Physical properties underlying observed kinematics of satellite galaxies

Radosław Wojtak¹ and Gary A. Mamon²

¹*Dark Cosmology Centre, Niels Bohr Institute, University of Copenhagen, Juliane Maries Vej 30, DK-2100 Copenhagen Ø, Denmark*

²*Institut d'Astrophysique de Paris (UMR 7095: CNRS and UPMC), 98 bis Bd Arago, F-75014 Paris, France*

9 July 2012

ABSTRACT

We study the kinematics of satellites around isolated galaxies selected from the Sloan Digital Sky Survey (SDSS) spectroscopic catalog. Using a model of the phase-space density previously measured for the halos of Λ CDM dark matter cosmological simulations, we determine the properties of the halo mass distribution and the orbital anisotropy of the satellites as a function of the colour-based morphological type and the stellar mass of the central host galaxy. We place constraints on the halo mass and the concentration parameter of dark matter and the satellite number density profiles. We obtain a concentration-mass relation for galactic dark matter haloes that is consistent with predictions of a standard Λ CDM cosmological model. The number density profile of the satellites appears to be shallower than of dark matter, with the scale radius typically 1.6 times larger than of dark matter. The orbital anisotropy around red hosts exhibits a mild excess of radial motions, in agreement with the typical anisotropy profiles found in cosmological simulations, whereas blue galaxies are found to be consistent with an isotropic velocity distribution. Our new constraints on the halo masses of galaxies are used to provide analytic approximations of the halo-to-stellar mass relation for red and blue galaxies.

Key words: galaxies: kinematics and dynamics – cosmology: dark matter

1 INTRODUCTION

According to the standard Λ CDM cosmological model, the majority of the total energy density of the Universe is deposited in the form of dark energy and dark matter (Komatsu et al. 2011; Rozo et al. 2010). The former is a homogeneously distributed component responsible for the observed acceleration of the Universe expansion, whereas the latter is highly clumped, setting up a base for the growth of cosmic structures. Dark matter (hereafter, DM) assembles within quasi-spherical haloes that host cosmological objects of all scale, from dwarf galaxies to clusters of galaxies. The properties of such haloes are one of the most fundamental predictions of the current cosmological model. As first discovered by Navarro, Frenk, & White (1995, 1996), and confirmed in many more recent and much better-resolved cosmological simulations (e.g. Springel et al. 2005, 2008; Klypin et al. 2011), a key feature of DM haloes is the universal shape of their (hereafter NFW) density profile, whose logarithmic slope varies from -1 in the centre to -3 at large radii, while the transition scale between these two slopes is correlated with the halo mass (Navarro et al.

1997; Ludlow et al. 2011). This property is the subject of various observational tests at all halo masses.

Studying the properties of DM distribution in galactic haloes is a challenge. Most methods rely on tracers whose positions coincide with the stellar component. Therefore, they probe only the inner part of an underlying gravitational potential of DM halo on the scale of a few per cent of the virial radius. Common means to study the inner part of DM density profiles is the measurement of rotation curves for spiral galaxies (Sofue & Rubin 2001), the line-of-sight velocity dispersion profiles of stars (Bertin et al. 1994; Cappellari et al. 2006) or planetary nebulae (e.g., Napolitano et al. 2011), strong (Koopmans et al. 2006) and weak lensing (Mandelbaum et al. 2006a; Gavazzi et al. 2007) or X-ray observations (Humphrey et al. 2006) for early type galaxies. The main difficulty in interpretation of these data arises from the fact that the mass of DM is comparable to the baryonic component and, therefore, constraints on DM mass profile depends critically on the mass estimate of the stellar component (Mamon & Lokas 2005a). In particular, the uncertainty of stellar population models, when applied to elliptical galaxies, leads unavoidably to an

ambiguity about the shape of DM density profile (e.g., Grillo 2012).

There are only two methods that allow to measure the DM distribution at distances comparable to the virial radius of the halo: weak lensing and kinematics of satellite galaxies.¹ Due to a very weak signal per galaxy, both methods rely on stacking the data, giving insight into the properties of a spherically averaged rather than individual haloes.

Lensing analyses were successfully applied to measure projected mass profiles in galactic haloes. Most results are consistent with a universal NFW (Navarro, Frenk, & White 1997) density profile of dark matter and the mass-concentration relation emerging from cosmological simulations of a standard Λ CDM model (Mandelbaum et al. 2006a, 2008). Nevertheless, one weak lensing study (Gavazzi et al. 2007) concludes to a shallower DM density profile at large radii around massive elliptical galaxies, even slightly shallower than the singular isothermal sphere model with $\rho \propto r^{-2}$. Moreover, strong lensing studies of ellipticals also point to a density profile with slope very close to -2 between 0.3 and $0.9 R_e$ (Koopmans et al. 2006, 2009).² However, the naïve superposition of NFW DM and the observed Sersic (1968) model for the stars, leads to a slope close to -2 (from the model of Mamon & Lokas 2005b, we predict a slope of -2.2 ± 0.1 in the range studied by Koopmans et al.): the stars dominate the mass profile within $\approx 2 R_e$ (Mamon & Lokas 2005b), but at large radii the NFW DM component should dominate and the slope should be considerably steeper than -2 ($\simeq -2.6$ at the virial radius from the model above).

Satellite kinematics provide a popular means to estimate halo masses. Because host galaxies possess a very small number of observable satellites, usually one or two, one must stack the satellites over many host galaxies. Still, early attempts (Zaritsky, Smith, Frenk, & White 1993; Zaritsky & White 1994) suffered from their small sample sizes. The Sloan Digital Sky Survey (SDSS) is the first very large spectroscopic sample of galaxies with accurate redshifts and digital photometry for a credible analysis of satellite kinematics. McKay et al. (2002) estimated host galaxy masses out to a fixed radius using $M(r_{\text{ap}}) = C r_{\text{ap}} \sigma_{\text{ap}}^2(r_{\text{ap}})/G$, where $C = d \ln \nu / d \ln r$ is a constant determined by fitting a power-law to the stacked satellite surface density profile. Brainerd & Specian (2003) perform a similar analysis on the 2dFGRS, where they measure the line-of-sight (LOS) velocity dispersion by fitting the LOS velocity distribution by a Gaussian plus a constant term for interlopers (instead of simply removing the high-velocity interlopers). They were the first to obtain M/L as a function of luminosity, and both for red and blue hosts. But their analysis suffered from the relatively inaccurate velocities and photometry of the 2dFGRS. Prada et al. (2003) were the first to notice a decline of LOS velocity dispersion at projected radii. They showed that the distribution of satellites in projected phase space (PPS) is consistent with the expectations from Λ CDM. Conroy et al. (2007) analysed the

satellites from the Data Release 4 (DR4) of the SDSS and from the DEEP2 survey at $z \approx 1$, again with a model for the interlopers, and were the first to derive the variation of virial mass with host galaxy luminosity, separating red and blue galaxies. They found that red host galaxies of given blue luminosity have double the halo mass as their blue counterparts. More et al. (2011) added a second Gaussian to the Gaussian+flat distribution of LOS velocities and fit aperture velocity dispersions (which are less sensitive than LOS velocity dispersions to the unknown orbital anisotropy and its radial variation) to find a halo versus stellar mass in close agreement with that of Conroy et al.

Unfortunately, all these analyses have flaws. For example, they all assume that the LOS velocity distribution is a Gaussian (generally plus a uniform interloper distribution), while it is known that anisotropic velocities lead to non-Gaussian LOS velocities (Merritt 1987). Thus by taking into account the non-Gaussian nature of the LOS velocity distribution (see also Amorisco & Evans 2012), one can both obtain more accurate constraints on the mass profile and derive constraints on the orbital anisotropy.

We (Wojtak et al. 2009) have recently developed a self-consistent method to derive at the same time the mass and velocity anisotropy profiles of spherical systems. Our method is based on the fact that the distribution of objects in PPS is a triple integral (Dejonghe & Merritt 1992) over the LOS and the two plane-of-sky velocities of the six-dimensional distribution function (DF) parameterized in terms of energy and angular momentum that Wojtak et al. (2008) measured on the halos of a Λ CDM simulation. This approach gives much deeper insight into the data than tests of consistency shown before. It allows for a self-consistent comparison between a set of physical parameters determined from cosmological simulations and observations. Furthermore, analysis based on a PPS model does not rely on data binning which always introduces an artificial signal smoothing.

This manuscript is organised as follows. In section 2, we describe the data and criteria for selecting isolated galaxies and their satellites. Section 3 presents our dynamical model and a method of constraining parameters of the systems. The results of data analysis and discussion are presented in section 4. The summary and a discussion follow in section 5. In this work, we adopted a flat Λ CDM cosmological model with $\Omega_m = 0.3$ and $H_0 = 70 \text{ km s}^{-1} \text{ Mpc}^{-1}$.

2 DATA

We made use of the Sloan Digital Sky Survey Data Release Seven (SDSS DR7, Abazajian et al. 2009) to select isolated galaxies and the satellite galaxies orbiting them. To search for the host galaxies, we considered a volume-limited subsample of the spectroscopic part of the survey defined by an r -band Petrosian absolute magnitude threshold $M_r = -19.0$ and redshift range of $3000 \text{ km s}^{-1} < cz < 25000 \text{ km s}^{-1}$. The apparent magnitudes were converted to the absolute scale assuming k -correction based on an analytical approximation provided by Chilingarian, Melchior, & Zolotukhin (2010).

We defined isolated central galaxies as those that are brighter by ΔM than every other galaxy lying inside an observational cylinder of a projected radius ΔR and a line-of-

¹ Strong lensing is typically restricted to inner regions, while X-ray measurements extend only to about half the virial radius.

² We call R_e the effective radius, containing half of the luminosity in projection.

sight velocity range $2\Delta v_{\text{los}}$. We fixed all fiducial parameters at values defining a rather restrictive criterion for galaxy isolation: $\Delta M > 1.505$ (corresponding to the flux ratio of at least 2), $\Delta R < 1$ Mpc and $\Delta v_{\text{los}} < 1500$ km s⁻¹ (for comparison, see McKay et al. 2002; Prada et al. 2003; van den Bosch et al. 2004; Conroy et al. 2007; Klypin et al. 2011). All galaxies lying in the cylinder and that are dimmer than the magnitude threshold are considered to be the satellites of the central galaxies. Due to a rather wide velocity cut-off, some of them are galaxies of background or foreground (interlopers). Disentangling between these two classes of galaxies is an intrinsic part of data analysis described in the following section.

We split the sample of the selected host galaxies into red and blue galaxies using $g - r + 0.017M_r$ colour diagnostic (see Roche et al. 2010), where g and r are k -corrected Petrosian magnitudes. A boundary value of this diagnostic was fixed at 0.25 which is a minimum of the colour distribution lying between two Gaussian components corresponding to two galaxy populations. Using the publicly available catalog of the stellar mass estimates from the SDSS DR7,³ we found the masses of the stellar component of all central galaxies. Stellar masses were estimated using Bayesian approach as outlined in Kauffmann et al. (2003), with fitting the observed photometry as described in Salim et al. (2007). The model assumed initial mass function of Chabrier (2003). We neglected 8 per cent of host galaxies for which stellar mass estimates were not available.

Our final sample consists of 8800 and 2600 satellites around 3800 red and 1600 blue hosts, respectively. The host galaxies cover the stellar mass range from $\log_{10}(M_*/M_\odot) = 10.0$ to $\log_{10}(M_*/M_\odot) = 11.8$ for red galaxies and from $\log_{10}(M_*/M_\odot) = 9.5$ to $\log_{10}(M_*/M_\odot) = 11.0$ for the blue ones. Since the stellar mass is a better indicator of the haloes mass than galaxy luminosity (More et al. 2011), we split the sample of the host galaxies into several bins of the stellar mass. We used 6 and 3 bins for the red and blue hosts, respectively, as indicated in Table 1. This procedure guarantees that the kinematic sample in every bin represents a homogeneous sample of DM haloes.

3 INFERENCE OF PHYSICAL PARAMETERS

The velocity distribution of satellite galaxies is mostly determined by the gravitational potential of DM haloes of the central galaxy. The second factor is the orbital anisotropy describing the fraction of radial-to-tangential orbits in the system. This additional degree of freedom makes data analysis more complex due to a well-known fact of the mass-anisotropy degeneracy (Binney & Mamon 1982; Merrifield & Kent 1990). Breaking this degeneracy requires using rather complicated models accounting for higher-order corrections to the Jeans equation (e.g., Merrifield & Kent 1990; Lokas 2002; Lokas & Mamon 2003; Wojtak et al. 2009). On the other hand, the advantage is that the same data allow to study two physical properties of the host-satellites systems at the same time – mass distribution of

DM halo and the orbital structure of the satellites (e.g., Lokas & Mamon 2003; Lokas 2009; Wojtak & Lokas 2010).

We analysed the kinematic data in terms of the projected phase-space density, i.e. the density of satellite galaxies on the plane spanned by the line-of-sight velocity v_{los} and the projected distance from the host galaxy R . Due to projection effects, the $v_{\text{los}} - R$ plane is populated by the true physical satellite galaxies of the central galaxies as well as interlopers. We did not apply any interloper removal to the data, but rather we accounted for the presence of interlopers in a statistical sense as an inherent part of a proper analysis. This approach is particularly justified in case of the composite kinematic data for which the phase-space distribution of interlopers is smooth enough to be modelled by a continuous probability function, and is commonly adopted in many studies on kinematics of satellite galaxies (Prada et al. 2003; Conroy et al. 2007; Klypin & Prada 2009). The probability describing the phase-space distribution of interlopers introduces an additional degree of freedom to the proper model associated with the physical properties of the host-satellites systems. The observed projected phase-space density $p_{\text{los}}(R, v_{\text{los}})$ may be expressed as the following sum

$$g(R, v_{\text{los}}) = (1 - p_i) g_s(R, v_{\text{los}}) + p_i g_i(R, v_{\text{los}}), \quad (1)$$

where $g_s(R, v_{\text{los}})$ and $g_i(R, v_{\text{los}})$ are the projected phase-space densities of satellite galaxies and interlopers respectively, and p_i is the probability of a randomly picked galaxy being an interloper.

3.1 Phase-space density model

As a model of the phase-space distribution of satellite galaxies, we used an anisotropic model of the distribution function developed by (Wojtak et al. 2008). The model was designed to describe the phase-space properties of simulated DM haloes and it was successfully utilised to constrain mass profile and the orbital anisotropy in nearby galaxy clusters (Wojtak & Lokas 2010). The only modification required to adjust the model to the new context of systems of hosts and satellites is a non-constant ratio of DM-to-tracer density profile. Constant mass-to-light ratio appears to be a robust assumption in galaxy clusters (Biviano & Girardi 2003; Lokas & Mamon 2003), but it is not justified for the systems of satellite galaxies for which observations point to a bias between spatial distribution of DM and the satellite (Guo et al. 2012).

Following (Wojtak et al. 2008), we considered the phase-space density $f(\mathbf{r}, \mathbf{v})$ of the following form

$$f(\mathbf{r}, \mathbf{v}) = f_E(E) L^{-2\beta_0} \left(1 + \frac{L^2}{2L_0^2} \right)^{(\beta_0 - \beta_\infty)}, \quad (2)$$

where E and L are positively defined binding energy and angular momentum per unit mass, β_0 and β_∞ are the asymptotic values of the anisotropy parameter at small and large radii, respectively. The anisotropy parameter quantifies the orbital anisotropy in terms of the ratio of the radial-to-tangential velocity dispersion and is traditionally defined as

$$\beta(r) = 1 - \frac{\sigma_r^2(r)}{2\sigma_t^2}, \quad (3)$$

where σ_r and σ_t are the velocity dispersions in radial and tangential direction, respectively. The angular momentum

³ <http://www.mpa-garching.mpg.de/SDSS/DR7/Data/stellarmass.html>

part of the distribution function (2) is a generalisation of a well-know $L^{-2\beta}$ ansatz for systems with a constant anisotropy parameter (Hénon 1973). It permits a wide family of the anisotropy profiles, suitable for constraining not only a global degree of the anisotropy, but also its radial profile. The anisotropy profiles are monotonic functions changing between two asymptotic values with the radius of transition given by L_0 parameter (see Wojtak et al. 2008, for details).

The energy part of the distribution function (2) is related to the density profile of satellite galaxies $\rho_s(r)$ and an underlying absolute value of the gravitational potential $\Psi(r)$ through the following integral equation

$$\rho_s(r) = \iiint f_E(E) L^{-2\beta_0} \left(1 + \frac{L^2}{2L_0^2}\right)^{(\beta_0 - \beta_\infty)} d^3v, \quad (4)$$

where $E = \Psi(r) - \frac{1}{2}v^2$ is the binding energy. The mass profile at large distances from the central galaxies is dominated by DM. While the stars can contribute up to half the mass at $5 R_e$ (see upper right panel of Fig. 4 of Mamon & Lokas 2005b), we choose to neglect the contribution of stars (or in other words to assume that they are distributed like the DM). We checked that this assumption has negligible effect on our analysis (see Discussion).

We also approximated the DM density profile by the universal NFW profile (Navarro et al. 1997) for which the gravitational potential takes the following form (Cole & Lacey 1996; Lokas & Mamon 2001)

$$\Psi(r) = \Psi_0 \frac{\ln(1 + r/r_s^{\text{DM}})}{r/r_s^{\text{DM}}}, \quad (5)$$

where r_s^{DM} is the scale radius at which logarithmic slope of DM density profile equals to -2 . Our choice of the NFW parameterisation is motivated not only by cosmological simulations, but also by observational results showing consistency between satellite kinematics and dynamical predictions for DM haloes with the NFW density profile (Prada et al. 2003; Klypin et al. 2011). We note that the Ψ_0 and r_s^{DM} are the principal parameters in the analysis which can be easily converted into more popular quantities describing the mass profile of DM haloes such as the virial mass or the concentration parameter (see Lokas & Mamon 2001 for all equations needed for parameter transformations).

The number density profile of satellite galaxies may be effectively approximated by the NFW profile with a scale radius unrelated to the concentration of DM (e.g., Guo et al. 2012). This property is independent of morphological type and the stellar mass of the host galaxy. Following this observational motivation, we adopted

$$\rho_s(r) \propto \frac{1}{(r/r_s^{\text{sat}})(1 + r/r_s^{\text{sat}})^2}, \quad (6)$$

as the number density of the satellites, where r_s^{sat} is a new scale radius.

Having specified $\rho_s(r)$ and $\Psi(r)$ one can solve equation (4) for the energy part of the distribution function. As shown by Wojtak et al. (2008), the integral over velocity space may be reduced to a one-dimensional problem. Then, the resulting integral equation may be inverted numerically. We used the same scheme of the integral inversion as outlined in Wojtak et al. (2008). Although the algorithm was designed to work for a single-component system with an

NFW density profile, we checked that it is also feasible in case of two-component systems.

The projected phase-space density of satellite galaxies in (1) was obtained by integrating the full phase-space density (2) over velocities \mathbf{v}_\perp perpendicular to the line of sight and a spatial coordinate z parallel to the line of sight (Dejonghe & Merritt 1992)

$$g(v_{\text{los}}, R) = 2\pi R \int dz \iint d^2v_\perp f(E, L). \quad (7)$$

Following the scheme outlined by Wojtak et al. (2009), we calculated this integral numerically using Gaussian quadrature. We did not apply any fiducial truncation to the distance along the line of sight keeping the upper limit of the corresponding integral as defined by the condition of positive binding energy, i.e. $E = \Psi(\sqrt{R^2 + z^2}) - v_{\text{los}}^2/2 \geq 0$.

For interlopers, we adopted a uniform projected phase-space distribution, i.e. $g_i \propto R$. It has been demonstrated that this model effectively separates gravitationally bound members of the central system from interlopers whose velocities are mostly dominated by the Hubble flow (Wojtak et al. 2007; Mamon, Biviano, & Murante 2010).

As a consistency check, we verified the robustness of this model by comparing it with the distribution of galaxies at $R > 100$ kpc and $1000 \text{ km s}^{-1} < |v_{\text{los}}| < 1500 \text{ km s}^{-1}$, which constitutes a clear subsample of interlopers for all bins of the stellar mass ($|v_{\text{los}}|$ exceeds maximum escape velocity at all halo masses as large as $10^{13.5} M_\odot$). Although the surface density of these galaxies is consistent with a uniform distribution, the velocity distribution for massive red hosts appears to exhibit a weak and broad non-uniform component. We attribute this feature to an environmental effect: massive red galaxies, although selected by the same isolation criteria, tend to populate denser environment which enhances the number of interlopers relative to low-density environments behind and in front of the host galaxy. Consequently, interloper density decreases with increasing velocity $|v_{\text{los}}|$. We found that in order to account for this effect it suffices to consider the following modification of a uniform model

$$g_i \propto R \left\{ (1 - p_g) + p_g \frac{1}{\sqrt{2\pi}\sigma_g} \exp\left[-\frac{v_{\text{los}}^2}{2\sigma_g^2}\right] \right\}, \quad (8)$$

where $\sigma_g = 500 \text{ km s}^{-1}$ and p_g is a nuisance parameter defining relative weight of the Gaussian component. This form of g_i was used only for three bins of the most massive red host galaxies with $\log_{10}(M_*/M_\odot) > 11.0$.

3.2 Incompleteness

Spectroscopic survey of the SDSS is not complete on angular scales smaller than $55''$ imposed by the minimum separation of the fibers in the spectrograph (Blanton et al. 2003). The limit of the completeness corresponds to the physical scale of 92 kpc at the maximum redshift defining the sample of isolated galaxies. This distance is a substantial fraction of the virial radius and, therefore, it is relevant to correct the projected phase-space density model for the incompleteness. The correction was incorporated by means of weighting the projected phase-space density according to the local value of the completeness $w(R)$

$$\hat{g}(R, v_{\text{los}}) = [g(R, v_{\text{los}})]^{1/w(R)}. \quad (9)$$

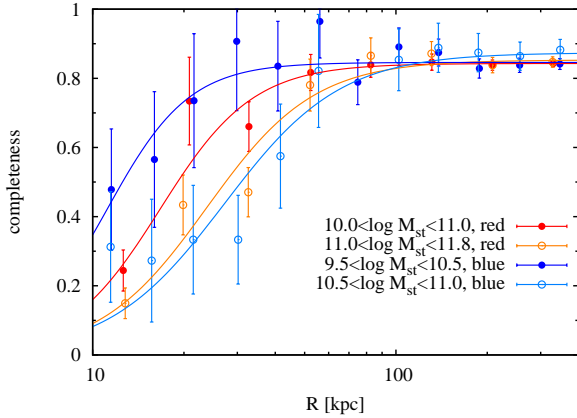


Figure 1. Completeness of the SDSS redshift survey around isolated host galaxies. The data points are the measured values of completeness, obtained by comparing the counts of SDSS spectroscopic and photometric data. The colours represent different stellar mass bins of red and blue host galaxies as indicated in the legend.

We measured the completeness of the data by computing the ratio of the surface number density of galaxies with spectroscopic redshifts to the surface density of all galaxies brighter than the magnitude limit of the SDSS spectroscopic survey, i.e. $r = 17.7$ in r -band of Petrosian magnitude (see Fig. 1). In order to account for a redshift dependence we split the sample of red and blue galaxies into two bins of the stellar mass corresponding to two classes of the absolute magnitude. We found that the completeness may be well fitted by the following analytical form

$$w(R) = w_0 \frac{(R/R_w)^\alpha}{1 + (R/R_w)^\alpha}, \quad (10)$$

where w_0 , R_w and α are free parameters. We fitted this profile to the data in all mass bins of the host galaxies. The resulting best-fit profiles of $w(R)$ (see solid lines in Fig. 1) were used as the final weighting function in (9). The final procedure of parameter inference was positively tested on incomplete mock data generated from the distribution function with a uniform background of interlopers.

3.3 Parameter estimation

We made use of kinematic data of satellite galaxies to place constraints on parameters of DM mass profile and the orbital anisotropy. For this, we adopted a Bayesian approach, maximising the likelihood of the distribution of satellites in PPS. The likelihood function \mathcal{L} was defined as

$$\begin{aligned} \ln \mathcal{L} &= \sum_{j=1}^N \ln \hat{g}(R_j, v_{\text{los } j} | \mathbf{a}), \\ &= \sum_{j=1}^N \frac{1}{w(R_j)} \ln g(R_j, v_{\text{los } j} | \mathbf{a}), \end{aligned} \quad (11)$$

where the sum is over all satellite galaxies in a given stellar mass bin of the host galaxies and \mathbf{a} is a vector of the model parameters. Both g_s and g_i are normalised to 1 over the area confined by velocity cut-off $|v_{\text{los}}| < 1500 \text{ km s}^{-1}$ and radius range $[R_{\text{min}}, R_{\text{max}}]$. As the maximum radius R_{max} ,

we used the virial radius (see next paragraph) as it determines a natural boundary of the equilibrated part of DM haloes. Since the virial radius is a function of some model parameters, its value was estimated in an iterative approach starting with the best initial guess based on the halo-stellar-mass relation provided by Dutton et al. (2010). For the most massive host galaxies, we imposed an additional limit $R_{\text{max}} < 400 \text{ kpc}$ which prevented from including the satellites which may be common to the host galaxy and local group or cluster of galaxies. We also imposed a minimum radius, because 1) our correction to the spectroscopic incompleteness is uncertain at small radii where our measured completeness is low, and 2) because photometric pipelines such as that of the SDSS tend to fragment large (host) galaxies into one big one and many small ones surrounding it, that appear like satellites, but are HII regions or spiral arms instead. The minimum radius R_{min} was fixed at 5 effective radii for red galaxies and 15 kpc for the blue ones. Effective radii were estimated independently for every stellar mass bin using a scaling relation with the stellar mass found by Hyde & Bernardi (2009). The resulting minimum radius R_{min} changes from 10 kpc for $\log_{10}(M_*/M_\odot) = 10.0 - 10.5$ to 55 kpc for $\log_{10}(M_*/M_\odot) = 11.5 - 11.8$.

The maximisation of the likelihood was carried out using the Markov Chain Monte Carlo (MCMC) technique with the Metropolis-Hastings algorithm (Gelman et al. 2004, see e.g.). The set of the primary parameters used in the MCMC analysis comprises the scale radius r_s^{sat} of the number density of satellites (6), the dimensionless $r_s^{\text{sat}}/r_s^{\text{DM}}$ ratio, the normalisation Ψ_0 of the gravitational potential (5), the asymptotic velocity anisotropy at small and large radii (β_0 and β_∞ , respectively), the interloper probability p_i in (1) and the relative weight p_g of the Gaussian part in the velocity distribution (8) of interlopers (applied only to the data of red galaxies with $M_* > 10^{11} M_\odot$). We determined constraints on the mass profiles by converting parameters of the gravitational potential, i.e. Ψ_0 and r_s^{DM} , into the standard parameters characterising DM halo with the universal NFW density profile: the virial mass M_Δ and the concentration parameter c_Δ . The virial mass is defined in terms of the mean density inside the sphere of radius r_Δ (the so-called virial radius) relative to the critical density ρ_c

$$\frac{3M_\Delta}{4\pi r_\Delta^3} = \Delta \rho_c, \quad (12)$$

where Δ is the virial overdensity. The concentration parameter is the virial radius expressed in the unit of the scale radius r_s^{DM} , i.e. $c_\Delta = r_\Delta/r_s^{\text{DM}}$. We adopted two commonly used values of the overdensity parameter: $\Delta = 200$ and $\Delta = 100$. The latter corresponds, to a 3 per cent precision, to the virial overdensity of a standard Λ CDM cosmological model (Bryan & Norman 1998).

We carried out the MCMC analysis assuming log-uniform priors for r_s^{sat} , Ψ_0 and $r_s^{\text{sat}}/r_s^{\text{DM}}$, and uniform priors for all remaining parameters. We fixed L_0 (eq. [2]) at $0.2\sqrt{\Psi_0}r_s^{\text{sat}}$ corresponding to the $\sim 1 r_s^{\text{sat}}$ transition radius between two asymptotic values of the anisotropy parameter (Wojtak & Lokas 2010). The central anisotropy β_0 was limited by $\beta_0 < 1/2$ in order to prevent distribution function from taking negative values (An & Evans 2006). Constraints on all parameters are based on Markov chains containing 2×10^4 models in every bin of the stellar mass.

$\log_{10}(M_\star[M_\odot])$	$\log_{10}(M_{100}[M_\odot])$	c_{100}	$\log_{10}(M_{200}[M_\odot])$	c_{200}	$r_{\text{s(sat)}}/r_{\text{s(DM)}}$	$N_{\text{sat}}/N_{\text{host}}$
10.00 – 10.50(red)	$12.26^{+0.03}_{-0.22}$	$11.9^{+19.0}_{-7.4}$	$12.19^{+0.03}_{-0.20}$	$8.9^{+14.7}_{-5.8}$	$1.7^{+3.0}_{-1.2}$	128/105
10.50 – 10.75(red)	$12.40^{+0.05}_{-0.08}$	$16.7^{+8.5}_{-8.9}$	$12.34^{+0.04}_{-0.08}$	$12.7^{+6.6}_{-6.9}$	$4.0^{+3.7}_{-1.6}$	303/242
10.75 – 11.00(red)	$12.58^{+0.02}_{-0.05}$	$10.6^{+5.5}_{-3.6}$	$12.51^{+0.03}_{-0.05}$	$7.9^{+4.3}_{-2.8}$	$3.4^{+1.6}_{-1.4}$	740/524
11.00 – 11.25(red)	$12.87^{+0.03}_{-0.07}$	$5.6^{+5.3}_{-2.4}$	$12.78^{+0.03}_{-0.06}$	$4.1^{+4.1}_{-1.8}$	$1.4^{+1.3}_{-0.6}$	1072/645
11.25 – 11.50(red)	$13.19^{+0.07}_{-0.10}$	$2.6^{+2.5}_{-1.4}$	$13.04^{+0.10}_{-0.09}$	$1.8^{+1.9}_{-1.1}$	$0.8^{+0.9}_{-0.4}$	726/357
11.50 – 11.80(red)	$13.68^{+0.06}_{-0.40}$	$6.9^{+15.5}_{-5.6}$	$13.60^{+0.09}_{-0.30}$	$5.1^{+12.1}_{-4.2}$	$1.5^{+4.3}_{-1.2}$	248/72
9.50 – 10.00(blue)	$11.82^{+0.13}_{-0.43}$	$16.1^{+16.6}_{-15.0}$	$11.76^{+0.10}_{-0.42}$	$12.2^{+12.9}_{-11.5}$	$1.9^{+2.3}_{-1.7}$	44/42
10.00 – 10.50(blue)	$12.07^{+0.06}_{-0.13}$	$7.4^{+4.5}_{-4.3}$	$11.99^{+0.06}_{-0.11}$	$5.5^{+3.5}_{-3.3}$	$1.6^{+1.4}_{-1.0}$	159/142
10.50 – 11.00(blue)	$12.41^{+0.05}_{-0.12}$	$4.5^{+3.7}_{-2.6}$	$12.30^{+0.06}_{-0.10}$	$3.3^{+2.8}_{-2.0}$	$1.3^{+1.4}_{-0.7}$	323/263

Table 1. Constraints on the parameters of DM density profile and the number density of galaxy satellites in all bins of the stellar mass and both types of host galaxies (red and blue): DM halo mass M_{100} (or M_{200}), the concentration parameter c_{100} (or c_{200}) and the ratio of tracer-to-DM scale radius $r_{\text{s(sat)}}/r_{\text{s(DM)}}$. The table provides the best fit values at the maximum of the posterior probability and the ranges containing 68 per cent of the corresponding marginal probability. The last column contains the number of satellites between R_{min} and R_{max} , N_{sat} , and the number of hosts, N_{host} .

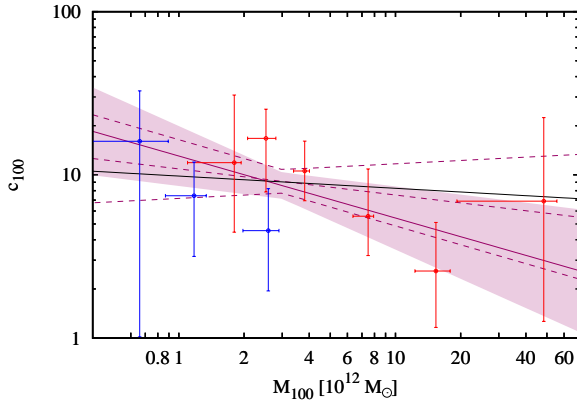


Figure 2. Concentration-mass relation for galaxy-size haloes. The points with the error bars show constraints on the halo mass and the concentration parameter of the DM density profile inferred from the kinematics of the satellite galaxies. The purple line is the best-fit power-law fit and the shaded region is the 1σ confidence area resulting from propagating the errors on the slope and the normalisation (dotted lines show the best-fit profile and the 1σ confidence area when neglecting the most outlying point at $M_{100} = 1.5 \times 10^{13} M_\odot$). The black solid line is the median concentration-mass relation from cosmological simulations of a standard Λ CDM model (the Bolshoi Simulation, Klypin et al. 2011).

Every chain was preceded by a number of trial chains ran to estimate the covariance matrix of the proposal probability distribution (Gelman et al. 2004).

4 RESULTS

4.1 Mass profile

Table 1 contains constraints on the halo mass, the concentration parameter and the ratio of the tracer-to-dark-matter scale radius of the density profile, for all bins of the host galaxies. Independently of the halo mass and the colour of the hosts, the concentration parameter appears to be fairly well constrained with a typical value ≈ 10 . This is a plausible signature that DM density profile is steeper than r^{-2} at large radii ($r > r_{100}/10$) and shallower at small radii.

Fig. 2 shows the comparison between our ‘observational’ constraints on the concentration-mass relation from satellite kinematics (red and blue points) and its theoretical predictions (black solid line). For the latter, we plotted the concentration-mass profile from the Bolshoi Simulation – a high resolution simulation of a standard Λ CDM cosmological model with the most updated cosmological parameters (Klypin et al. 2011). The concentration parameters inferred from the satellite velocities are fairly consistent with the profile from cosmological simulations. However, our constraints are not tight enough to determine robustly the slope of the mass-concentration relation. Power-law fits to the data of both types of the host galaxies, with symmetrised errors, yields the slope -0.38 ± 0.22 (purple solid line in Fig. 2) or -0.16 ± 0.22 (purple dashed line in Fig. 2) when neglecting the most outlying point at $M_{100} = 1.5 \times 10^{13} M_\odot$. This is consistent with the predicted value of -0.075 (Klypin et al. 2011) as well as with a flat profile. The best-fit normalisation at $M_{100} = 3 \times 10^{12} M_\odot$ is 8.6 ± 1.8 when fitting to all data points, and 9.1 ± 1.6 when excluding the outlier, in excellent agreement with the concentration $c_{100} = 9.1$ from the simulations of the current Λ CDM cosmological model (Klypin et al. 2011).

Since the data appear not to reveal a statistically significant dependence of the concentration parameter on the halo mass, we combined constraints on the concentration

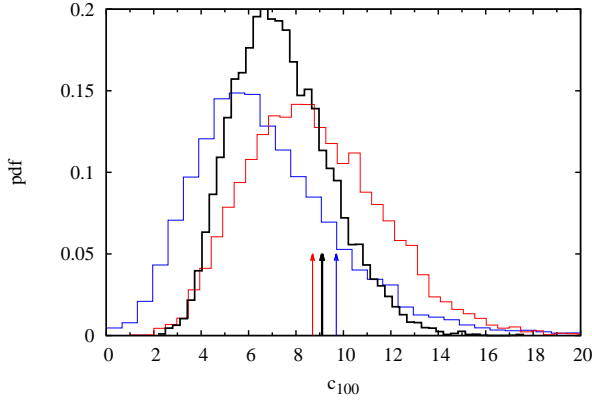


Figure 3. Probability distribution for the concentration parameter of DM density profile, as combined from all bins of the stellar mass. The arrows indicate the median concentration parameters of simulated DM haloes (Klypin et al. 2011) corresponding to the median halo mass in red, blue and both types of the central galaxies. Red, blue and black colours correspond to the red and blue host galaxies, and both types of the central galaxies.

from all bins of the stellar mass. Fig. 3 shows the resulting posterior probability distribution for red, blue and both types of the host galaxies. The concentration parameter of DM haloes hosting red galaxies is fully consistent with the predictions of DM cosmological simulations corresponding to the same range of the halo masses (red arrow). DM density in haloes of blue galaxies appears to be slightly less concentrated compared to theoretical expectation (blue arrows). This deviation, however, is not statistically significant (around 1σ) and it may be easily verified in future with the use of more data from upcoming redshift surveys. Combining results from all bins of the stellar mass yields the typical concentration parameter $8.0^{+3.1}_{-2.6}$ for red galaxies, $5.7^{+3.2}_{-2.4}$ for the blue ones and $6.8^{+2.2}_{-1.8}$ for both types.

Fig. 4 shows probability distribution for $r_s^{\text{sat}}/r_s^{\text{DM}}$ combined from all bins of the stellar mass. Typical scale radius of the satellite number density profiles around red host galaxies is larger by factor of $1.8^{+0.9}_{-0.6}$ than that corresponding to DM ($r_s^{\text{sat}}/r_s^{\text{DM}} > 1.0$ at the 97 per cent confidence level). This finding confirms previous studies based on photometric data from the SDSS and showing that the spatial distribution of the satellite around red galaxies is more extended than of DM and is well-fitted by the NFW profile with the concentration parameter typically 2 times smaller than that expected for DM (Guo et al. 2012). Constraints on the ratio of the satellite-to-dark-matter scale radius for blue galaxies do not point to any bias between the spatial distribution of DM and the satellites, i.e. $r_s^{\text{sat}}/r_s^{\text{DM}} = 1.4^{+0.8}_{-0.6}$. Combining the results from both types of central galaxies yields the host-independent ratio $r_s^{\text{sat}}/r_s^{\text{DM}} = 1.6^{+0.5}_{-0.3}$ ($r_s^{\text{sat}}/r_s^{\text{DM}} > 1.0$ at the 97 per cent confidence level). This estimate is fully consistent with the bias between the concentration parameters of the subhalo number density profile and dark matter density profile measured in cosmological simulations, $r_s^{\text{sat}}/r_s^{\text{DM}} = 1.5$ from the Millennium Simulation (Sales et al. 2007) and $r_s^{\text{sat}}/r_s^{\text{DM}} = 1.3$ from the Bolshoi Simulation (Klypin et al. 2011).

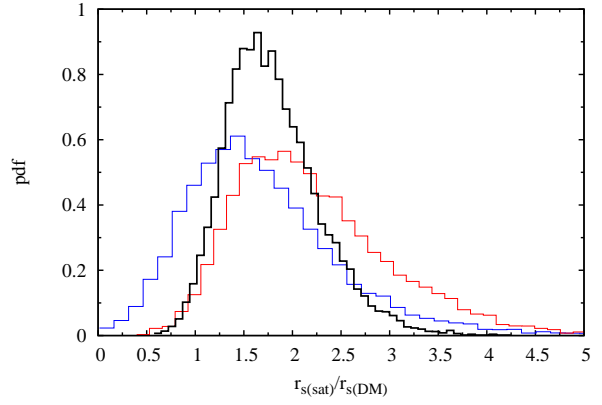


Figure 4. Probability distribution for $r_s^{\text{sat}}/r_s^{\text{DM}}$ combined from all bins of the stellar mass, where r_s^{sat} and r_s^{DM} are the scale radii of the satellite number density profile and dark matter density profile. Red, blue and black colours correspond to the red and blue host galaxies, and both types of the central galaxies.

4.2 Halo-stellar mass relation

Fig. 5 shows the halo mass as a function of the stellar mass of both types of host galaxies. The halo mass is measured with accuracy up to 0.05 dex for red galaxies with stellar masses $\log_{10}(M_*/M_\odot) = 10.75 - 11.25$ for which number of the satellites per stellar mass bin reaches maximum. Obtained constraints on the halo-stellar mass relation reveal a change of the slope between low and high stellar masses, with the transition mass $\log_{10}(M_*/M_\odot) \approx 11$. Following Dutton et al. (2010), we find that a reasonable fit to the data is achieved using the following function

$$M_{200} = M_{h0} \left(\frac{M_*}{M_{*0}} \right)^a \left[\frac{1}{2} + \frac{1}{2} \left(\frac{M_*}{M_{*0}} \right)^\gamma \right]^{(b-a)/\gamma}, \quad (13)$$

where α and β are the logarithmic slopes at small and large stellar masses, respectively, M_{*0} and M_{h0} are the stellar and halo mass at the transition point, and γ is a parameter controlling the sharpness of the transition. Fitting this function to the data of red galaxies yields $a = 0.29$, $b = 2.91$, $\gamma = 1.24$, $\log_{10}(M_{*0}/M_\odot) = 11.3$ and $\log_{10}(M_{h0}/M_\odot) = 13.1$. Constraints on the halo-to-stellar mass relation for blue galaxies cover approximately one order of magnitude in the stellar mass and are consistent with a power-law profile with the logarithmic slope 0.66 ± 0.07 and the normalisation $\log_{10}(M_{200}/M_\odot) = 12.0$ at the stellar mass $\log_{10}(M_*/M_\odot) = 10.3$.

We compare our results with empirical profiles obtained by Dutton et al. (2010) as a compilation of all observational constraints on the halo-stellar mass relation available in the literature (see shaded stripes in Fig. 5). The widths of the profiles correspond to the 2σ credibility range, where σ is the error dominated by systematics related to differences between various mass measurements based on weak lensing (Mandelbaum et al. 2006b, 2008; Schulz et al. 2010) or satellite kinematics (Conroy et al. 2007; More et al. 2011), and dashed lines represent the best fit profiles. We find that the halo-stellar mass relation from our analysis of red galaxies is fairly consistent with other measurements. It only exhibits a sharper transition between low and high stellar

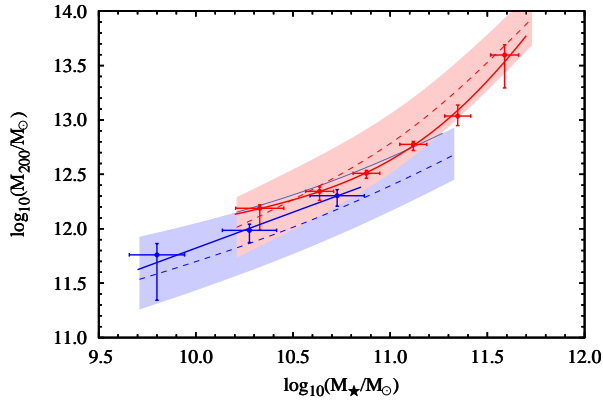


Figure 5. Relation between the halo mass M_{200} and the stellar mass M_{\star} for red and blue galaxies (red and blue colour, respectively). The error bars indicate the range containing 68 per cent of the marginal probability distribution for the halo mass and the scatter of the stellar masses in bins. Solid lines are the best fit power-law profile for blue galaxies and the best fit double-power-law profile given by (13) for red galaxies. Shaded stripes and dashed lines show halo-stellar mass relation representing a compilation of results available in the literature (Dutton et al. 2010). The widths of the stripes correspond to the 2σ credibility range and the dashed line is the best fit double-power-law profile.

mass regime and a slightly shallower profile at small stellar masses.

The halo-stellar mass relation for blue galaxies appears to be offset by 0.15 dex towards higher halo masses, although the trend is not statistically significant. We note, however, that our reference profile plotted (Dutton et al. 2010) represents a compilation of a quite heterogeneous sample of measurements which are incidentally obtained mostly from satellite kinematics. Closer inspection of Fig. 1 in Dutton et al. (2010) shows that most of the halo masses lie above the best-fit profile. In particular, halo masses obtained by Conroy et al. (2007) and More et al. (2011) are offset by 0.20 dex and 0.1 dex respectively which are sufficiently large values to match our measurement of the halo masses. It appears that the halo-stellar mass relation for blue galaxies found by Dutton et al. (2010) is biased towards lower halo masses, probably as a result of special selection of data points used for fitting.

4.3 Anisotropy of the satellite orbits

Constraints on the anisotropy parameter obtained in individual bins of the stellar mass are not tight enough to draw any solid conclusion. For example, working in separate bins of host stellar mass, we cannot differentiate between an isotropic velocity distribution ($\beta = 0$) and the typical anisotropy profile found in simulated DM haloes where β increases with radius from 0.1 in the halo centre to 0.3–0.5 at the virial radius (Wojtak et al. 2005; Ascasibar & Gottlöber 2008; Cuesta et al. 2008). Since there is no theoretical hint that the anisotropy may depend on the halo mass and results obtained in different stellar mass bins do not reveal any trend with the stellar mass, it is advisable to combine constraints from all bins into one.

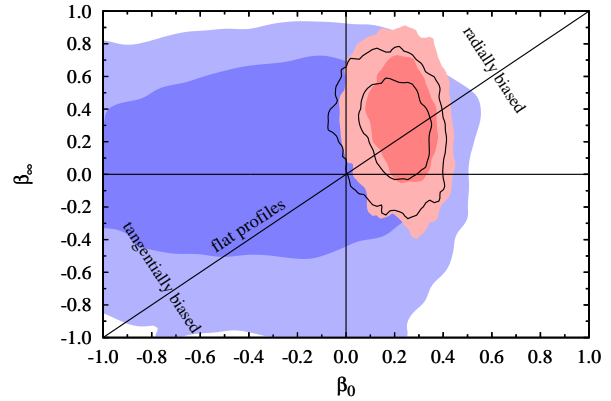


Figure 6. Constraints on the asymptotic values of the anisotropy profile parameter $\beta(r)$, $\beta_0 = \beta(r \ll r_s^{\text{sat}})$ and $\beta_{\infty} = \beta(r \gg r_s^{\text{sat}})$. The contours are the confidence regions containing 68 and 95 per cent of the probability combining results from the stellar mass bins. Red, blue and black colours correspond to red, blue and both types of host galaxies.

Fig. 6 shows contours of the resulting joint probability distribution of two parameters determining the anisotropy profile, $\beta_0 = \beta(r \ll r_s^{\text{sat}})$ and $\beta_{\infty} = \beta(r \gg r_s^{\text{sat}})$. When we combine all host galaxy mass bins, we find that the satellite orbits are mildly radially anisotropic with $\beta_0 = 0.2 \pm 0.1$ and $\beta_{\infty} = 0.3 \pm 0.2$, in fair agreement with the predictions from cosmological simulations as well as with the universal relations between the anisotropy and the logarithmic slope of an underlying DM density profile (Hansen & Moore 2006; Hansen et al. 2010). The shift between the marginal probability distributions for β_{∞} and β_0 may indicate a tendency for the anisotropy to increase with radius. This effect, however, is of a marginal statistical significance and the data still permit a flat anisotropy profile.

Our measurement of the anisotropy parameter relies mostly on the data for red galaxies (compare the red and black probability distributions in Fig. 6). Combining results for red galaxies yields $\beta_0 = 0.26^{+0.08}_{-0.10}$ and $\beta_{\infty} = 0.38^{+0.26}_{-0.27}$ which are statistically consistent with the constraints obtained for both types of central galaxies. Measurement of the orbital anisotropy around blue galaxies is much weaker due to significantly smaller number of the satellites and it does not allow to differentiate between an isotropic velocity distribution and the anisotropy profile motivated by cosmological simulations (see the blue probability distribution in Fig. 6). The analysis of the combined probability distribution results in $\beta_0 = -0.2^{+0.4}_{-0.6}$ and $\beta_{\infty} = 0.2^{+0.3}_{-0.5}$.

5 SUMMARY AND DISCUSSION

We made use of satellite kinematics compiled from the redshift catalog of the SDSS to measure the physical properties of dark matter haloes and the orbital anisotropy of the satellites orbiting fairly isolated galaxies. Data analysis was carried out in the framework of the projected phase-space density based on an anisotropic model of the distribution function for equilibrated spherical systems. This approach

avoids arbitrary binning the data. It furthermore allows us to break the mass-anisotropy degeneracy.

The concentration parameter of DM density profiles has a typical value of ≈ 9 , in full consistency with the results from cosmological simulations (Klypin et al. 2011). We did not find statistically significant differences between DM concentrations in red and blue galaxies. Our constraints on the concentration-mass relation are not tight enough to determine its slope over the range of galactic halo masses. However, a more robust measurement of the $c - M_{100}$ slope may be achieved by means of complementing these results by similar constraints at higher halo masses available in the literature. Combining the normalisation of the $c - M_{100}$ resulting from satellite kinematics with that obtained by Wojtak & Lokas (2010) from galaxy kinematics in clusters ($c_{100} = 6.8 \pm 0.7$ at $M_{100} = 4.9 \times 10^{14} M_{\odot}$) yields the slope -0.05 ± 0.04 , in fair agreement with -0.075 from cosmological simulations (Klypin et al. 2011).

Although our analysis relies on a specific parameterisation of the density profile, the existence of a well-constrained dark matter scale radius $r_s^{\text{DM}} < r_{100}$ suffices to conclude that the observed satellite kinematics is fully compatible with the NFW density profile of DM and can hardly be reconciled with an isothermal sphere model suggested in several studies based on lensing analysis of massive elliptical galaxies (Koopmans et al. 2006, 2009; Gavazzi et al. 2007). An isothermal density profile of DM would noticeably affect the measurement of the concentration parameter resulting in $r_s^{\text{DM}} \approx r_{100}$. This finding confirms and complements a number of tests showing consistency of satellite kinematics with the NFW profile of DM density (Prada et al. 2003; Klypin & Prada 2009). It also contradicts results of some studies based on weak lensing analysis around massive elliptical galaxies and resulting in isothermal sphere density profile at radii dominated by DM, i.e. ≈ 100 effective radii (see e.g. Gavazzi et al. 2007). This apparent flattening of the density profile should probably be attributed to a projection effect of the local dense environment rather than to DM haloes.

In our analysis, by adopting a single NFW model for the host mass distribution, we have neglected the contribution of the stellar component. Since elliptical galaxies are known to be dominated by their stellar component within the effective radius (Mamon & Lokas 2005a; Humphrey et al. 2006), one may worry that our DM concentrations will be overestimated, even though we only considered satellites further than $5 R_e$ from the host galaxy. For example, the total density profile of a two-component NFW+Sérsic model is very close to a singular isothermal in the range $0.1 \rightarrow 1 R_e$ (see upper left panel of Fig. 4 of Mamon & Lokas 2005b), as also determined from strong lensing analyses in a similar range of projected radii (Koopmans et al. 2006). Since the mass distribution returned from our model is most sensitive to the line-of-sight velocity dispersion profile, $\sigma_{\text{los}}(R)$, we asked ourselves how much lower would the DM concentration be if we incorporated a Sérsic (1968) model to the mass distribution.

We performed this test for our red host galaxies. For each of our bins of stellar mass, we determined the median r -band absolute magnitude, then obtained from Table 3 of Simard et al. (2011) the effective radii, R_e , and Sérsic indices, n , for these absolute magnitudes, after restricting the

SDSS sample of Simard et al. to the Red Sequence (using the same cut as we did in our mass analysis) and our adopted redshift range. We then computed $\sigma_{\text{los}}(R)$ for the satellite population with a two-component NFW+Sérsic mass model, adopting the central stellar mass of our mass bin with the values of R_e and n that we obtained above, the satellite scale radius that we previously measured (derived from Table 1), adopting $\beta(r) = 0.2$ for the satellites (consistent with Fig. 6), as well as the DM normalisation derived from our 1-component mass model (Table 1). The DM concentration, c_{100} , is a free parameter. We iterated on c_{100} until our profile of $\sigma_{\text{los}}(R)$ matched the profile expected for a 1-component NFW model. For each of the six mass bins, we were then able to match $\sigma_{\text{los}}(R)$ to better than 0.5 per cent between $5 R_e$ and the virial radius r_{100} . In the end, we found that the concentration of the DM component was 7 to 20 per cent lower than in the 1-component model. This suggests that our derived values of c_{100} are overestimated by 7 to 20 per cent. Note that if we allowed for adiabatic contraction (e.g., Gnedin et al. 2011), the DM concentration would be greater, hence our overestimate would be lower. This simple analysis suggests that our choice of a single NFW model for the mass distribution of isolated galaxies beyond $5 R_e$ is reasonable, as the predicted line-of-sight velocity dispersion profiles match that of more realistic two component models and our concentration is typically overestimated by only 10 per cent.

Satellite kinematics reveals a bias between the spatial distributions of DM and satellite galaxies. The scale radius of the satellite number density profile is typically larger by factor of 1.6 than of DM. This finding is consistent with the estimate of a counterpart bias between DM particles and subhaloes found in cosmological simulations (see e.g. Sales et al. 2007; Klypin et al. 2011). We did not find any statistically significant difference between the bias of red and blue galaxies.

The orbital anisotropy of satellite galaxies exhibits a mild excess of radial orbits with typical anisotropy parameter $\beta = 0.2 \pm 0.1$ in the inner regions and $\beta = 0.3 \pm 0.2$ in the outer regions of their hosts. These constraints on the inner and outer asymptotic values of the anisotropy profile are too weak to reveal any statistically significant trend of the anisotropy with radius. Due to the substantial difference between the numbers of satellites around red and blues hosts, our constraints on the orbital anisotropy come principally from the satellites around red hosts. This radial anisotropy around red (giant elliptical) galaxies has been predicted from hydrodynamical simulations of binary mergers (Dekel et al. 2005). Some giant elliptical galaxies shows signs of such radial outer anisotropy (Das et al. 2008; de Lorenzi et al. 2008), while other do not (Napolitano et al. 2011). In fact, our asymptotic value for the anisotropy, $\beta_{\infty} = 0.3 \pm 0.2$, suggests that satellites have less radial orbits than the particles at analogous radii within Λ CDM haloes. The velocity distribution of the satellites orbiting blue galaxies is consistent with an isotropic model.

ACKNOWLEDGMENTS

The Dark Cosmology Centre is funded by the Danish National Research Foundation. RW is grateful for the hospital-

ity of Institut d'Astrophysique de Paris where part of this work was done. RW thanks Steen Hansen for fruitful discussions and Anna Gallazzi for her useful advice about stellar masses of galaxies from SDSS. The computations were performed on the facilities provided by the Danish Center for Scientific Computing.

REFERENCES

- Abazajian K. N. et al., 2009, *ApJS*, 182, 543
 Amorisco N. C., Evans N. W., 2012, *MNRAS*, accepted, arXiv:1204.5181
 An J. H., Evans N. W., 2006, *ApJ*, 642, 752
 Ascasibar Y., Gottlöber S., 2008, *MNRAS*, 386, 2022
 Bertin G. et al., 1994, *A&A*, 292, 381
 Binney J., Mamon G. A., 1982, *MNRAS*, 200, 361
 Biviano A., Girardi M., 2003, *ApJ*, 585, 205
 Blanton M. R. et al., 2003, *ApJ*, 592, 819
 Brainerd T. G., Specian M. A., 2003, *ApJ*, 593, L7
 Bryan G. L., Norman M. L., 1998, *ApJ*, 495, 80
 Cappellari M. et al., 2006, *MNRAS*, 366, 1126
 Chabrier G., 2003, *PASP*, 115, 763
 Chilingarian I. V., Melchior A.-L., Zolotukhin I. Y., 2010, *MNRAS*, 405, 1409
 Cole S., Lacey C., 1996, *MNRAS*, 281, 716
 Conroy C. et al., 2007, *ApJ*, 654, 153
 Cuesta A. J., Prada F., Klypin A., Moles M., 2008, *MNRAS*, 389, 385
 Das P. et al., 2008, *Astronomische Nachrichten*, 329, 940
 de Lorenzi F., Gerhard O., Saglia R. P., Sambhus N., De-
 battista V. P., Pannella M., Méndez R. H., 2008, *MNRAS*, 385, 1729
 Dejonghe H., Merritt D., 1992, *ApJ*, 391, 531
 Dekel A., Stoehr F., Mamon G. A., Cox T. J., Novak G. S., Primack J. R., 2005, *Nature*, 437, 707, arXiv:astro-
 ph/0501622
 Dutton A. A., Conroy C., van den Bosch F. C., Prada F.,
 More S., 2010, *MNRAS*, 407, 2
 Gavazzi R., Treu T., Rhodes J. D., Koopmans L. V. E.,
 Bolton A. S., Burles S., Massey R. J., Moustakas L. A.,
 2007, *ApJ*, 667, 176
 Gelman A., Carlin J. B., Stern H. S., Rubin D. B., 2004,
Bayesian Data Analysis. Chapman & Hall / CRC, Boca
 Raton
 Gnedin O. Y., Ceverino D., Gnedin N. Y., Klypin A. A.,
 Kravtsov A. V., Levine R., Nagai D., Yepes G., 2011, *ApJ*,
 submitted, arXiv:1108.5736
 Grillo C., 2012, *ApJ*, 747, L15
 Guo Q., Cole S., Eke V., Frenk C., 2012, *MNRAS*, submit-
 ted, arXiv:1201.1296
 Hansen S. H., Juncher D., Sparre M., 2010, *ApJ*, 718, L68
 Hansen S. H., Moore B., 2006, *New Astronomy*, 11, 333
 Hénou M., 1973, *A&A*, 24, 229
 Humphrey P. J., Buote D. A., Gastaldello F., Zappacosta
 L., Bullock J. S., Brighenti F., Mathews W. G., 2006, *ApJ*,
 646, 899
 Hyde J. B., Bernardi M., 2009, *MNRAS*, 394, 1978
 Kauffmann G. et al., 2003, *MNRAS*, 341, 33
 Klypin A., Prada F., 2009, *ApJ*, 690, 1488
 Klypin A. A., Trujillo-Gomez S., Primack J., 2011, *ApJ*,
 740, 102
 Komatsu E. et al., 2011, *ApJS*, 192, 18
 Koopmans L. V. E. et al., 2009, *ApJ*, 703, L51
 Koopmans L. V. E., Treu T., Bolton A. S., Burles S., Mous-
 takas L. A., 2006, *ApJ*, 649, 599
 Lokas E. L., 2002, *MNRAS*, 333, 697
 Lokas E. L., 2009, *MNRAS*, in press, arXiv:0901.0715
 Lokas E. L., Mamon G. A., 2001, *MNRAS*, 321, 155
 Lokas E. L., Mamon G. A., 2003, *MNRAS*, 343, 401
 Ludlow A. D., Navarro J. F., White S. D. M., Boylan-
 Kolchin M., Springel V., Jenkins A., Frenk C. S., 2011,
MNRAS, 415, 3895
 Mamon G. A., Biviano A., Murante G., 2010, *A&A*, 520,
 A30
 Mamon G. A., Lokas E. L., 2005a, *MNRAS*, 362, 95
 Mamon G. A., Lokas E. L., 2005b, *MNRAS*, 363, 705
 Mandelbaum R., Seljak U., Cool R. J., Blanton M., Hirata
 C. M., Brinkmann J., 2006a, *MNRAS*, 372, 758
 Mandelbaum R., Seljak U., Hirata C. M., 2008, *JCAP*, sub-
 mitted, arXiv:0805.2552
 Mandelbaum R., Seljak U., Kauffmann G., Hirata C. M.,
 Brinkmann J., 2006b, *MNRAS*, 368, 715
 McKay T. A. et al., 2002, *ApJ*, 571, L85
 Merrifield M. R., Kent S. M., 1990, *AJ*, 99, 1548
 Merritt D., 1987, *ApJ*, 313, 121
 More S., van den Bosch F. C., Cacciato M., Skibba R., Mo
 H. J., Yang X., 2011, *MNRAS*, 410, 210
 Napolitano N. R. et al., 2011, *MNRAS*, 411, 2035
 Navarro J. F., Frenk C. S., White S. D. M., 1995, *MNRAS*,
 275, 720
 Navarro J. F., Frenk C. S., White S. D. M., 1996, *ApJ*, 462,
 563
 Navarro J. F., Frenk C. S., White S. D. M., 1997, *ApJ*, 490,
 493
 Prada F. et al., 2003, *ApJ*, 598, 260
 Roche N., Bernardi M., Hyde J., 2010, *MNRAS*, 407, 1231
 Rozo E. et al., 2010, *ApJ*, 708, 645
 Sales L. V., Navarro J. F., Lambas D. G., White S. D. M.,
 Croton D. J., 2007, *MNRAS*, 382, 1901
 Salim S. et al., 2007, *ApJS*, 173, 267
 Schulz A. E., Mandelbaum R., Padmanabhan N., 2010,
MNRAS, 408, 1463
 Sersic J. L., 1968, *Atlas de galaxias australes*. Cordoba,
 Argentina: Observatorio Astronomico, 1968
 Simard L., Mendel J. T., Patton D. R., Ellison S. L., Mc-
 Connachie A. W., 2011, *ApJS*, 196, 11
 Sofue Y., Rubin V., 2001, *ARA&A*, 39, 137
 Springel V. et al., 2008, *MNRAS*, 391, 1685
 Springel V. et al., 2005, *Nature*, 435, 629
 van den Bosch F. C., Norberg P., Mo H. J., Yang X., 2004,
MNRAS, 352, 1302
 Wojtak R., Lokas E. L., 2010, *MNRAS*, in press,
 arXiv:1004.3771
 Wojtak R., Lokas E. L., Gottlöber S., Mamon G. A., 2005,
MNRAS, 361, L1
 Wojtak R., Lokas E. L., Mamon G. A., Gottlöber S., 2009,
MNRAS, 1120
 Wojtak R., Lokas E. L., Mamon G. A., Gottlöber S., Klypin
 A., Hoffman Y., 2008, *MNRAS*, 388, 815
 Wojtak R., Lokas E. L., Mamon G. A., Gottlöber S., Prada
 F., Moles M., 2007, *A&A*, 466, 437
 Zaritsky D., Smith R., Frenk C., White S. D. M., 1993,
ApJ, 405, 464

Zaritsky D., White S. D. M., 1994, ApJ, 435, 599